Dynamin A as a one-component division machinery for synthetic cells

De Franceschi, Nicola; Barth, Roman; Meindlhumer, Sabrina; Fragasso, Alessio; Dekker, Cees

DOI
10.1038/s41565-023-01510-3

Publication date
2023

Document Version
Final published version

Published in
Nature Nanotechnology

Citation (APA)
De Franceschi, N., Barth, R., Meindlhumer, S., Fragasso, A., & Dekker, C. (2023). Dynamin A as a one-component division machinery for synthetic cells. *Nature Nanotechnology*, *19*(1), 70-76. https://doi.org/10.1038/s41565-023-01510-3

nature nanotechnology

Article

https://doi.org/10.1038/s41565-023-01510-3

Dynamin A as a one-component division machinery for synthetic cells

Received: 5 December 2022

Accepted: 8 August 2023

Published online: 05 October 2023

Check for updates

Nicola De Franceschi[1,2], Roman Barth[1], Sabrina Meindlhumer[1], Alessio Fragasso[1] & Cees Dekker[1]

Membrane abscission, the final cut of the last connection between emerging daughter cells, is an indispensable event in the last stage of cell division and in other cellular processes such as endocytosis, virus release or bacterial sporulation. However, its mechanism remains poorly understood, impeding its application as a cell-division machinery for synthetic cells. Here we use fluorescence microscopy and fluorescence recovery after photobleaching measurements to study the in vitro reconstitution of the bacterial protein dynamin A inside liposomes. Upon external reshaping of the liposomes into dumbbells, dynamin A self-assembles at the membrane neck, resulting in membrane hemi-scission and even full scission. Dynamin A proteins constitute a simple one-component division machinery capable of splitting dumbbell-shaped liposomes, marking an important step towards building a synthetic cell.

The ability to divide is one of the most fundamental features of cellular life. Since a lipid membrane surrounds all cells, the division process necessarily entails a substantial membrane deformation. First, the mid-cell region of the cell is constricted, resulting in the formation of a so-called dumbbell-like shape, where a narrow neck still connects the two future daughter cells. In eukaryotes, this process is driven by an actomyosin ring[1], whereas constriction in bacteria is intracellularly coordinated by the Z-ring[2] with peptidoglycan synthesis occurring on the outer leaflet of the membrane[3]. Following constriction, the final step consists of membrane scission of the neck (also termed abscission). This is believed to be performed by other protein machinery such as the ESCRT-III complex in eukaryotes[4] and the evolutionary-related Cdv complex in Archaea[5]. It is not yet fully clear how abscission is accomplished in bacteria.

Membrane remodelling has been extensively studied in reconstituted systems[6]. Membrane abscission can be studied in various membrane geometries, that is, where proteins act from the outside on a membrane neck, or in a geometry where a membrane scission machinery acts from the inside of a membrane neck, the so-called 'reverse topology' (Extended Data Fig. 1)[7]. An example of the former is endocytosis, where eukaryotic dynamin binds to the outside of a membrane neck and induces the scission of endocytic pits[8]. Reverse-topology processes include scission events mediated by the ESCRT-III complex in eukaryotes[9], and cell division and sporulation in bacteria[10]. Recent years witnessed a growing interest in building a self-sustaining and self-reproducing synthetic cell[11]—a liposome filled with proteins that exhibits the features of natural cells. Cell division of such synthetic cells should occur in reverse topology as components of the division machinery need to be synthesized within the synthetic cell. However, such a division system has so far been missing[11].

In the filamentous bacteria *Streptomyces*, two GTPases, dynamin DynA and DynB, localize near a septum, where they induce the final stage of sporulation[12]. Although the exact function of DynA/B in *Streptomyces* remains incompletely understood, bacterial dynamin-like proteins have been widely associated with membrane-remodelling events[13]. For example, *Bacillus subtilis* DynA, which is a fusion protein that combines the functionalities of both DynA and DynB within one protein[14], has been shown to mediate Mg^{++}-dependent membrane fusion in vitro by binding to the headgroups of negatively charged lipids, whereas GTP hydrolysis was found to be dispensable for this process[15]. Moreover, DynA was shown to counteract stress-induced pores[16] during phage infections[17]. Notably, membrane scission and fusion involve the same 'topological reaction', but run in opposite directions—from one to two vesicles or vice versa. Inevitably, they both also entail the same hemi-scission/hemi-fusion intermediate state (Fig. 1a).

[1]Department of Bionanoscience, Kavli Institute of Nanoscience Delft, Delft University of Technology, Delft, The Netherlands. [2]IMol Polish Academy of Sciences, Warsaw, Poland. e-mail: c.dekker@tudelft.nl

https://doi.org/10.1038/s41565-023-01510-3

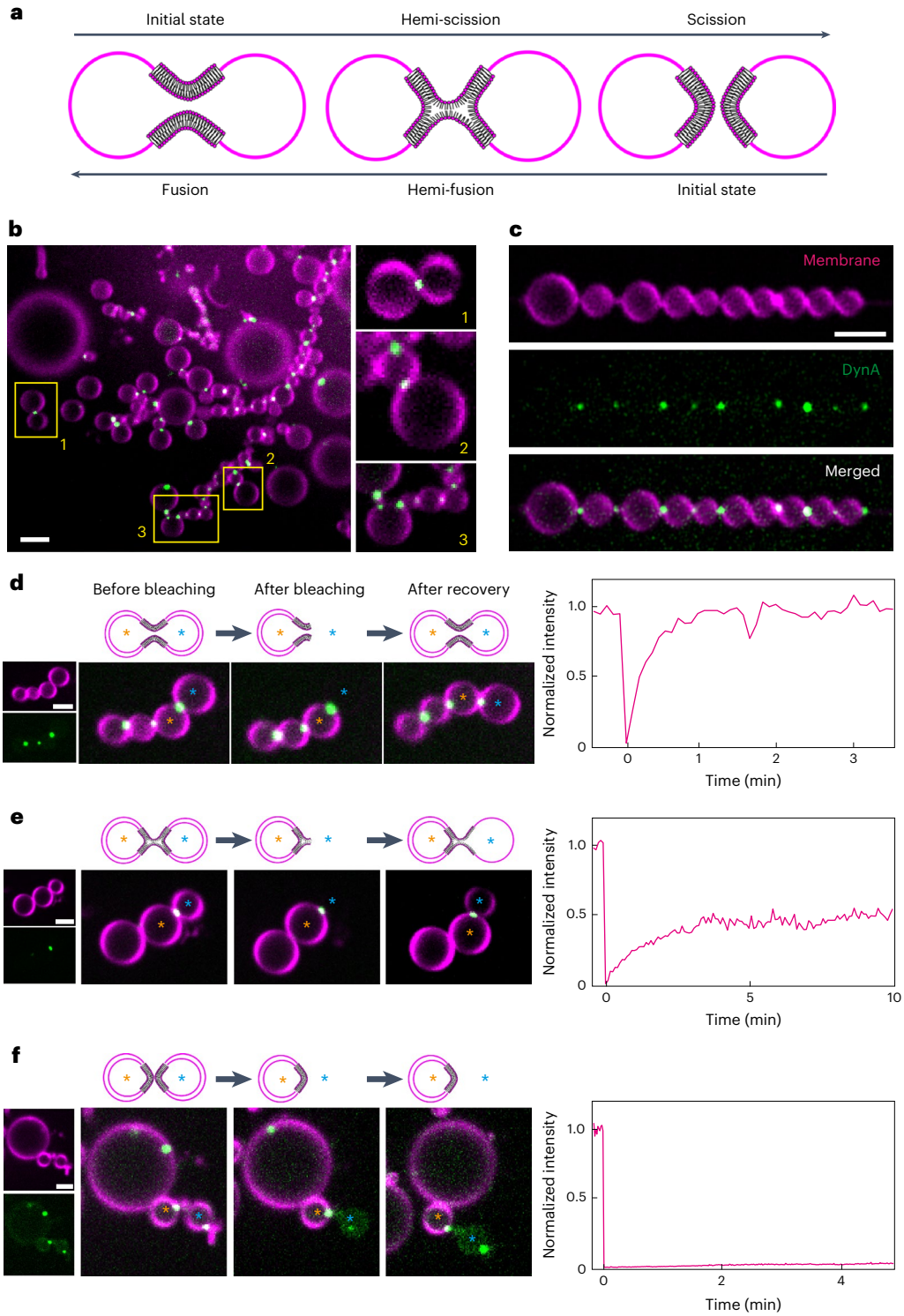

Fig. 1 | DynA localizes at the necks of dumbbells and affects membrane connectivity. a, Schematic depicting the fusion/scission 'topological reaction'. **b**, Large field of view of the preparation of dumbbells with encapsulated DynA generated with the SMS. The insets show detailed views of DynA clusters localized at the membrane necks. **c**, Example of a chain of dumbbells with DynA clusters at multiple necks. **d**, Full recovery of fluorescent lipids to a normalized intensity $N_I \approx 1$ upon photobleaching of one lobe of a chain of dumbbells. The bleached and control lobes are indicated by blue and orange asterisks, respectively. The right panel shows the normalized intensity (N_I) versus time. The schematic on top illustrates the membrane connectivity at the neck that is compatible with the recovery profile. **e**, Partial recovery of fluorescent lipids to a normalized intensity $N_I \approx 0.5$ upon photobleaching of a lobe of a chain of dumbbells. Colours, time trace and schematic are as in **a**. **f**, Absence of the recovery of fluorescent lipids upon photobleaching of a lobe of a chain of dumbbells. Colours, time trace and schematic are as in **a**. The gain in the DynA fluorescence channel was increased to show the continuous presence of the bleached lobe. Scale bars, 5 µm.

https://doi.org/10.1038/s41565-023-01510-3

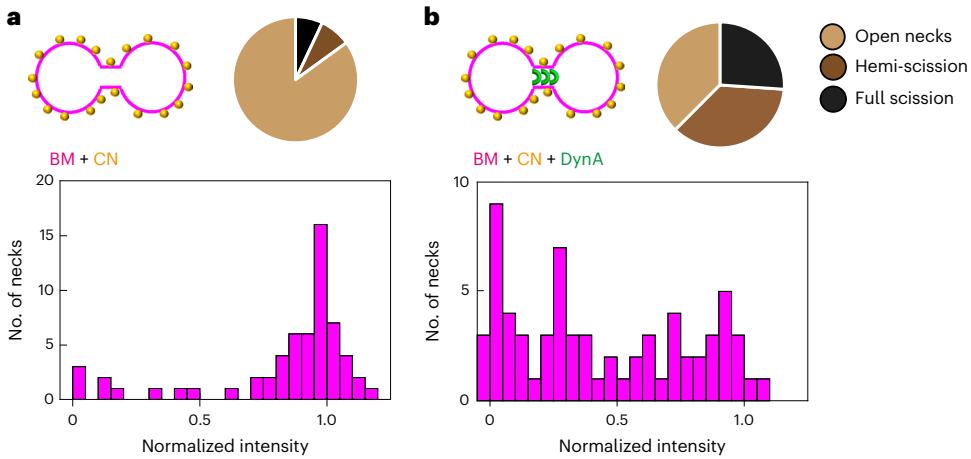

Fig. 2 | Quantification of membrane-remodelling events at necks in the presence or absence of DynA. a, Histogram of normalized intensities N_I for dumbbells with cholesterol–oligo and nanostars but without DynA (BM + CN; 60 necks from seven independent preparations). Pie chart indicating the fraction of open necks, hemi-scission and full scission events (top right). BM, bare membrane; CN, cholesterol–oligo + nanostars. **b**, Histogram of normalized intensities N_I for dumbbells with cholesterol–oligo, nanostars and DynA (BM + CN + DynA; 68 necks from 12 independent preparations). Pie chart indicating the fraction of open necks, hemi-scission and full scission events (top right).

Here we address the question of whether the bacterial *B. subtilis* DynA protein can mediate membrane scission when reconstituted inside membrane necks. We reconstituted recombinant DynA inside liposomes that were deformed into a dumbbell shape using the recently developed synthetic membrane shaper (SMS) approach[18]. Using fluorescence microscopy and fluorescence recovery after photobleaching (FRAP), we monitored whether soluble dyes within the liposomes and fluorescently labelled lipids in the bilayer leaflets could diffuse across the membrane neck. The experiments revealed that DynA localizes at the dumbbell neck, catalysing both membrane hemi-scission and full scission. Our data demonstrate a novel function for DynA and provide insights into the process of membrane scission in reverse topology, the biologically relevant geometry for cell division. Moreover, this dynamin-based single-protein system presents a simple synthetic divisome that is of interest for establishing division in synthetic cells[11].

DynA localizes at the neck of dumbbell liposomes

A high yield of dumbbell-shaped liposomes was obtained using the SMS technology that we recently introduced[18]. Often, 'chains of dumbbells' were generated, which are linear arrays of liposomes that are mutually connected by both membrane leaflets, forming a neck (similar to previously reported 'necklaces of pearls'[19]). These resulted from the shape transformation of a continuous membrane system during the process of liposome formation (Supplementary Video 1).

When DynA was included in the inner solution, a strong preferential localization of DynA was observed at the membrane necks in the resulting dumbbell structures (Fig. 1b), as evidenced by a bright fluorescent spot at the neck (Supplementary Video 2). In contrast, the binding of DynA to the liposome membrane outside the neck region was minimal. This indicates that DynA prefers to bind to highly curved membranes. For the present work, we focused on chains of dumbbells (Fig. 1c) as they present a useful framework to study the function of DynA at dumbbell necks in reverse topology.

DynA induces membrane remodelling

To probe the nature of membrane connectivity between lobes, we performed FRAP experiments, where the fluorescent lipids of one liposome within the chain were photobleached. The fluorescence intensity recovered over time as lipids flowed across the neck region that connected the adjacent lobes[18] (Fig. 1d–f). We quantified the degree of fluorescence recovery by the normalized intensity (N_I), which measures the ratio between the final fluorescence intensity of the bleached lobe after recovery and that of a neighbouring control lobe that was not photobleached (Supplementary Note 1, Extended Data Figs. 2 and 3 and Supplementary Fig. 1). This intensity N_I is normalized such that a final value of $N_I = 1$ indicates full recovery, whereas $N_I = 0$ signifies the absence of any recovery.

We observed three distinct outcomes of these FRAP experiments on liposome chains that were otherwise indistinguishable from each other. In some chains, full recovery occurred at $N_I = 1$ (Fig. 1d and Supplementary Video 3), indicating that both leaflets of the membranes of the two adjacent lobes were fully connected and supported lipid diffusion. This indicates the presence of an open neck, as confirmed by the control FRAP experiments on dumbbell-shaped liposomes without DynA, which yielded the same result (Extended Data Figs. 3b and 7a). A second set of data showed that even after a prolonged time, there was only a partial recovery that plateaued at N_I value somewhere between 0 and 1 (Fig. 1e and Supplementary Video 4). This is consistent with a scenario where hemi-scission had occurred, meaning that the inner leaflet of the membrane had undergone scission (thus preventing lipid diffusion across the neck), whereas lipids in the outer leaflet could still freely flow between the lobes, yielding a partial recovery of the fluorescence signal. Finally, some dumbbells displayed no recovery in FRAP experiments (Fig. 1f and Supplementary Video 5), consistent with a scenario where both leaflets had undergone scission. Even on full scission, we observed that the lobes did not detach from each other, most probably due to the presence of Mg^{++} ions in the outer buffer, which bridges negatively charged lipids in the membrane. However, in a few cases, we observed lobe detachment on scission (Extended Data Fig. 4).

DynA strongly increases the rate of hemi-scission and full scission

To discern to what extent these membrane (hemi-)scission events can be attributed to the action of DynA, we performed lipid FRAP experiments on chains of dumbbells ($n = 190$) that were generated by having either (1) only bare membrane (BM) or (2) cholesterol–oligo + nanostars on the outside (BM + CN) or (3) CN on the outside as well as DynA on the inside (BM + CN + DynA). Pooling all the data together yielded a plot for the normalized intensity N_I with three distinguishable populations that we fitted with Gaussians (Extended Data Fig. 5a). From fitting, we extracted mean values for the three populations that correspond to no lipid recovery (average $N_{I,1} = 0.04$, close to 0), partial recovery

https://doi.org/10.1038/s41565-023-01510-3

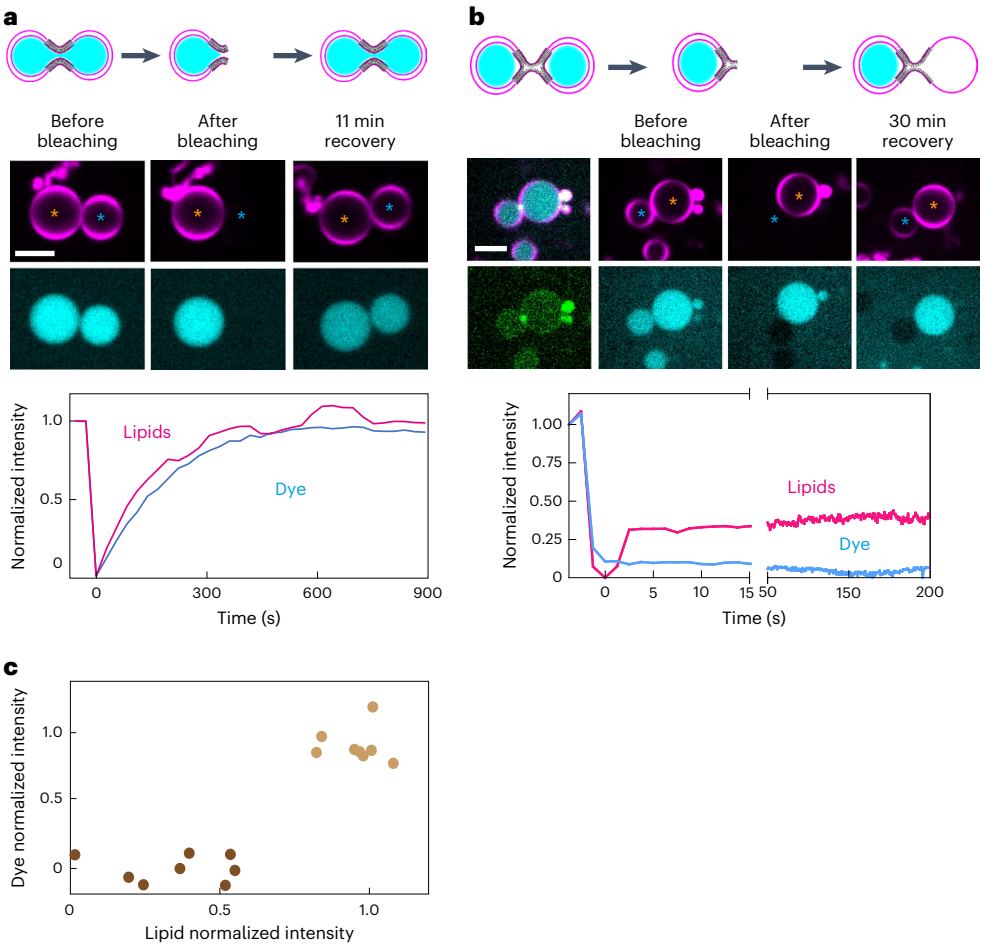

Fig. 3 | Characterization of DynA-induced membrane hemi-scission events. **a**, Concomitant FRAP of lipids and soluble dye in dumbbells in the absence of DynA. Normalized intensity versus time of both lipids and dye (bottom). **b**, Same data as **a**, but in the presence of DynA. **c**, Scatter plot showing the fraction of open necks, hemi-scission and full scission events based on lipid recovery and the corresponding recovery or absence of recovery of the soluble dye (n =16). The open necks are indicated in light brown; hemi-scission and scission events are indicated in dark brown. Scale bars, 5 µm.

(average $N_{l,2}$ = 0.31) and full recovery (average $N_{l,3}$ = 0.92, close to 1.00). Note that the $N_{l,2}$ = 0.31 peak is very close to the expected value of 0.33 for an ideal case of membrane hemi-scission (Supplementary Note 1 and Extended Data Fig. 2). The identification of these peaks with no scission (open neck), hemi-scission and full scission events, respectively, allowed us to quantify the number of these events in the different profiles for N_l for each experimental condition.

The vast majority (85%) of dumbbell liposomes formed by CN featured an open neck, as only a marginal increase in membrane hemi-scission (8%) and full scission (7%) events was observed (Fig. 2a), compared with dumbbells having only BMs that virtually showed all open necks (Extended Data Fig. 5b). This, however, strikingly changed upon the addition of DynA. The co-reconstitution of DynA on the inside and CN on the outside of chains of dumbbells resulted in 36% of necks in a hemi-scission state and 26% in a full scission state (Fig. 2b). This shows that DynA can induce both membrane hemi-scission and full scission in these conditions.

The presence of GTP seemed unnecessary for DynA-mediated membrane remodelling (Extended Data Fig. 6a), in agreement with the ability of DynA to mediate membrane fusion in a GTP-independent fashion[15]. However, the presence of Mg^{++} was required for DynA to bind the membrane (Extended Data Fig. 6b). DynA was furthermore found to narrow the neck, as measured for the subset of dumbbells where neither hemi-scission nor full scission occurred (Extended Data Fig. 6c).

DynA induces fusion of the inner leaflet that signals a hemi-scission state

To verify that the partial lipid recovery in FRAP experiments indeed corresponds to membrane hemi-scission, we encapsulated a soluble dye and performed the simultaneous photobleaching of lipids in the membrane and of the dye that was encapsulated in the lumen of the liposome. In the absence of DynA, dumbbells always exhibited full recovery of both lipids and soluble dye (Fig. 3a). This indicates that lipids and soluble dye could freely diffuse across the necks, as expected. In the presence of DynA, however, we often observed that on bleaching both dye and lipids, the lipids recovered only partially. In contrast, the soluble dye in the liposome's inner volume did not recover (Fig. 3b). This corroborates the presence of a hemi-scission state, which allows lipids from the outer leaflet to recover and while preventing both lipids of the inner leaflet and soluble dye from flowing across the neck.

We quantified the degree of recovery of both dye and lipids for each dumbbell, yielding the scatter plot shown in Fig. 3c. In about half of the dumbbells, we observed a full recovery of dye and lipids, indicating the presence of an open neck. In the remaining 50%, however, we observed either a partial lipid recovery or a total absence of lipid recovery, consistent with the hemi-scission and full scission data shown in Fig. 2. Importantly, in 100% of the cases in which the soluble dye did not recover, we observed either partial or a complete absence of lipid recovery. This correlation is expected for a closed neck, which prevents the dye from recovering. This can happen either by full scission

https://doi.org/10.1038/s41565-023-01510-3

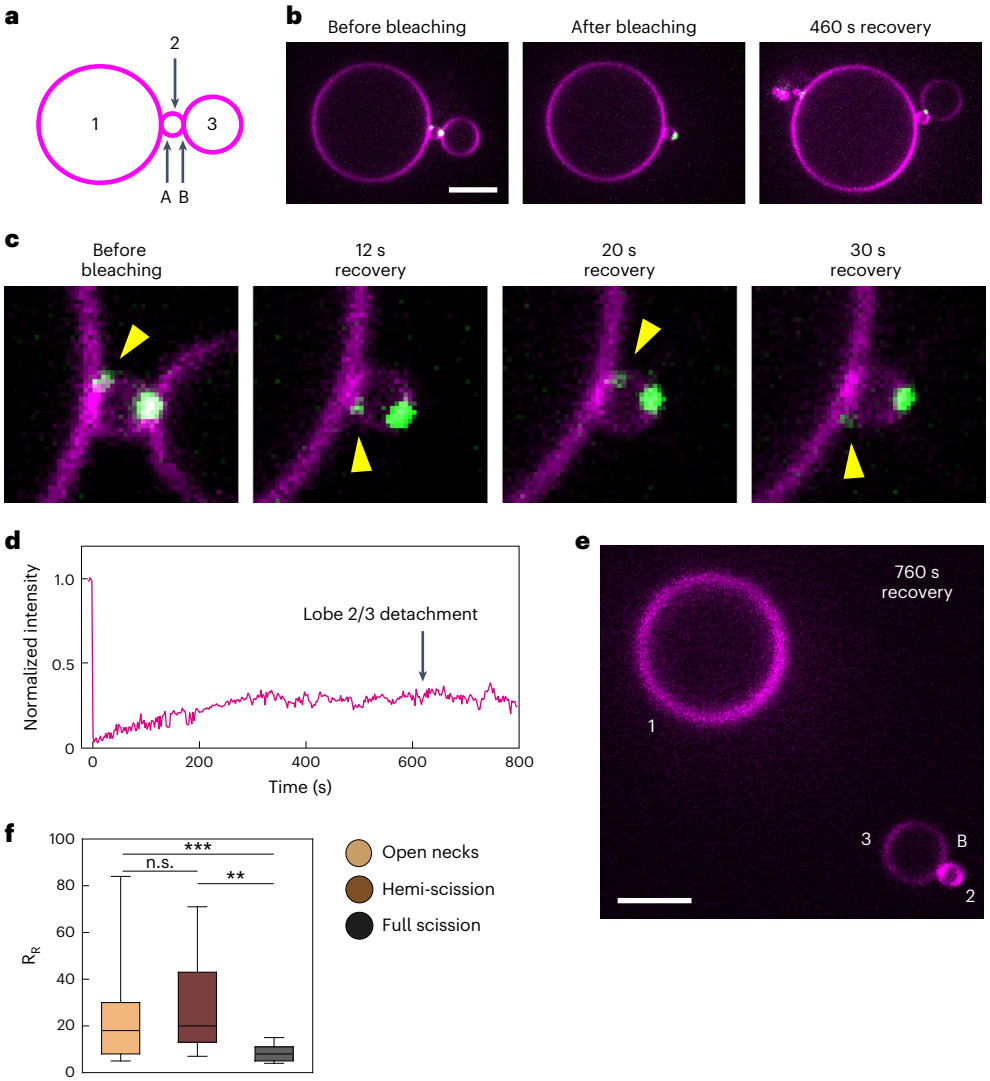

Fig. 4 | Example of a full scission event that was captured live. a, Schematic representing the dumbbell chain shown in **b**, composed of three lobes (called 1, 2 and 3) and two necks (called A and B). **b**, Lobe 3 was bleached in FRAP and subsequently underwent partial recovery, indicating that hemi-scission had occurred at neck B. Note that neck A must have stayed open, because lobes 1 and 2 exhibited a similar degree of fluorescence after recovery. Scale bar, 10 µm. **c**, Zoomed-in view of lobe 2 during the course of the FRAP experiment. A large DynA–D2 cluster was stably localized at neck B, whereas a smaller DynA–D2 cluster (indicated by the yellow arrowheads) was continuously diffusing on the inner surface of lobe 2 throughout the experiment. **d**, Fluorescence recovery trace of lobe 3. The recovery plateaued at about 300 s. The vertical arrow indicates the first frame in which lobe 2/3 was seen detaching from lobe 1 (that is, after 640 s of recovery). **e**, Microscopy image after 760 s showing that lobe 2/3 had drifted away by more than 30 µm from lobe 1. Note the large DynA–D2 cluster that was still stably localized at neck B, which remained in the hemi-scission state as inferred from the fluorescence levels of lobes 2 and 3. Scale bar, 10 µm. **f**, Recruitment ratio (R_R) of DynA. The line within the box is the median value. The lower and upper edges of the box represent the lower and upper quartiles, respectively, whereas the upper and lower lines indicate the maximum and minimal values of the data points. Here n =18 for open necks; n =12 for hemi-scission; n =14 for full scission. p = 0.35 for open necks versus hemi-scission; p = 0.006 for open necks versus full scission; p = 0.0004 for hemi-scission versus full scission using the Mann–Whitney U-test. Methods provide the calculation of R_R.

(in which case no lipid recovery is observed) or by hemi-scission (where scission of the inner leaflet would allow partial lipid recovery). The data, thus, confirm that partial lipid recovery corresponds to a hemi-scission state. We also confirmed that in the hemi-scission state, lipid recovery occurs by diffusion via the outer membrane leaflet. For this, we used fluorescently labelled CN, which was externally added and only bound the outer leaflet. Upon bleaching a dumbbell in the hemi-scission state, we observed that lipids partially recovered, whereas CN recovered fully (Extended Data Fig. 7a,b).

DynA from *B. subtilis* is a fusion protein composed of two halves, D1 and D2, with a similar domain architecture[14]. Both domains were found to mediate membrane fusion in vitro on their own, although with different efficiencies[14]. When reconstituted in our system, both D1 and D2 were found to localize at the necks of dumbbells (Extended Data Fig. 8a,b). Furthermore, both were found to be able to remodel membranes (Extended Data Fig. 8c). Still, they markedly differed in their efficiency, with D1 being more efficient at mediating hemi-scission and scission than D2. This may be due to a well-defined membrane binding patch in D1 (ref. 13), which may mediate strong lipid binding and thus favour membrane remodelling.

Full scission is mediated by smaller DynA clusters

Finally, we were able to capture a membrane-remodelling event live, which provides some hints on the mechanism of DynA-mediated remodelling (Supplementary Video 6). A dumbbell system composed of three lobes and two necks (Fig. 4a) exhibited two DynA–D2 clusters:

https://doi.org/10.1038/s41565-023-01510-3

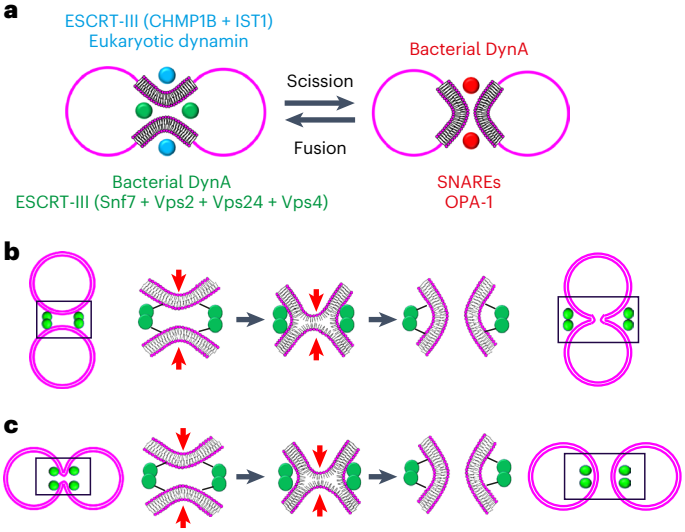

Fig. 5 | DynA in membrane scission and fusion. a, Schematic summarizing the proteins involved in membrane scission and fusion. The dots indicate the position of the proteins with respect to the membrane and colours correspond to the protein names listed. The membrane-remodelling activity of all these proteins has been confirmed by previous in vitro reconstitutions[15,31,34–37], whereas the scission activity of bacterial DynA is established here. **b**, Schematic representing membrane fusion via a hemi-fusion intermediate with DynA (in green) reconstituted on the outer leaflet. The black lines connecting the membrane with DynA indicate a physical interaction between the membrane and protein and clarify the ability of DynA to tether membranes in *trans*[38,39]. The red arrows indicate the direction of membrane deformation induced by DynA. **c**, Schematic representing membrane scission via a hemi-scission intermediate with DynA (in green) reconstituted on the inner leaflet.

a large cluster that was stably localized at neck B, and a smaller cluster that continuously diffused inside lobe 2 (Fig. 4b,c). Upon photobleaching of lobe 3, the data revealed that neck B, which was harbouring the larger cluster, was in a stable hemi-scission state (Fig. 4b,d,e). Fluorescence recovery of lobe 3 reached a plateau after about 5 min. Strikingly, about 11 min after bleaching, a spontaneous detachment of lobe 2/3 from lobe 1 was observed (Fig. 4d,e and Extended Data Fig. 9a,b), suggesting that neck A subsequently underwent full scission. These findings suggest that full membrane scission is mediated by a smaller mobile DynA cluster that only transiently engaged a pre-existing neck. The data imply that the efficiency of DynA-mediated full scission may be even larger than those reported in Figs. 2 and 3, because we preferentially probed necks that showed a stable cluster. The correlation between the degree of DynA enrichment and the propensity of the necks to undergo membrane rearrangement is consistent across the large dataset shown in Fig. 2. Full scission occurred more frequently when the degree of enrichment was relatively low ($R_R = 8 \pm 3$, $n = 14$, mean ± standard deviation), whereas it was more probable for the neck to be trapped in a hemi-scission intermediate when a higher amount of DynA was assembled to the neck ($R_R = 28 \pm 20$, $n = 12$, mean ± standard deviation) (Fig. 4f). This may indicate that excessive recruitment of DynA can impair the transition from hemi-scission to full scission.

Conclusions

Here we showed that bacterial DynA can trigger membrane scission when assembled inside membrane necks in dumbbell-shaped liposomes. With this demonstrated functionality, DynA adds to the family of membrane-remodelling proteins involved in fusion and scission (Fig. 5a). Previously, eukaryotic dynamin was shown to induce membrane scission when assembled on the outside of membrane nanotubes[20] and a hemi-scission intermediate was visualized[21]. The present work is the first example of the visualization of membrane hemi-scission triggered by a protein assembled inside membrane necks. Bacterial DynA was also shown to promote membrane fusion when assembled on the outer leaflet of liposomes in vitro[14]. Our work is the first demonstration of membrane scission activity by a bacterial member of the dynamin superfamily and, to the best of our knowledge, bacterial DynA is the only example of a protein able to trigger both membrane fusion and scission. DynA was previously suggested to tether membranes in *trans*[13], a configuration that—due to the symmetry of this topological reaction—can indeed explain liposome fusion as well as scission when DynA is present at the outside or inside, respectively (Fig. 5b,c).

Previous attempts to induce membrane scission in dumbbell systems relied on laser irradiation[22] or curvature induced by proteins bound to the outer leaflet[23]. In these reports, membrane scission was primarily established by observing the separation of daughter liposomes. It is, however, very common for liposomes to remain connected by lipid nanotubes, but such nanotubes are difficult to detect due to their intrinsic low fluorescence intensity (Extended Data Fig. 9c,d). Instead of apparent vesicle separation, we analysed dumbbells using FRAP, which is the more rigorous way to establish membrane connectivity. Furthermore, we performed experiments on linear chains of dumbbells, which originated from a single-membrane system (Supplementary Video 1). Such linear chains are unlikely to result from liposome adhesion, which would instead yield random aggregations.

Interestingly, at least half of the membrane-remodelling events triggered by DynA were arrested at the hemi-scission stage (Figs. 2b and 3b). We observed that the transition to full scission might be hindered by an excessive accumulation of DynA at the neck. In contrast, a small mobile cluster that only transiently engaged the neck could induce full scission (Fig. 4). Several other factors may contribute to the progression from hemi-scission to full scission. This transition can spontaneously occur when the neck is thin enough (<3 nm radius)[24,25]. In such a scenario, the role of DynA may be to merely reduce the neck width to such low diameters. Furthermore, the transition to full scission is favoured by membrane tension[26], and our setup with the SMS system induces a finite membrane tension[18] that may assist the (hemi-)scission action of DynA. The ability to visualize the hemi-scission intermediate is a unique feature of our approach that may be applied to other cellular processes where hemi-scission membrane is crucial, such as the biogenesis of lipid droplets[27].

The only other protein machinery that has been demonstrated to mediate membrane scission in an inverted topology is the eukaryotic ESCRT-III complex. This complex assembles inside membrane necks[28–30] and triggers full membrane scission[31] in in vitro tube-pulling assays. Notably, a hemi-scission intermediate was never visualized[4,32]. However, in these ESCRT experiments, the nanotube was kept under a pulling tension, facilitating scission, whereas potential hemi-scission intermediates probably became short-lived and hard to detect. The alternative methodology we have introduced based on the FRAP analysis of dumbbell liposomes allows discrimination between different membrane connectivity states, including hemi-scission. We found that DynA assembles in defined structures that laterally diffuse on the membrane to get captured by pre-existing necks where they can induce full scission. Such a behaviour was previously reported for the ESCRT-III protein CHMP2B. Upon reconstitution, CHMP2B was shown to quickly assemble into clusters that diffuse around the membrane to get captured by the neck[28]. The similarity between both systems may suggest a mechanism of membrane scission mediated by shape complementarity that may also be at play in the case of DynA.

In summary, we have shown that *B. subtilis* DynA promotes membrane scission in reverse topology, unveiling a new role for this protein. Due to its simplicity, this system presents an attractive candidate for building a divisome for synthetic cells[11]. A mainstream approach to

build a synthetic cell relies on using reconstituted transcription/translation systems to produce the proteins for growth and division[33]. Multicomponent systems such as ESCRT-III with defined stoichiometries complicate their implementation, whereas a divisome having fewer components is favoured. In this regard, a single-component system like DynA is an excellent choice for building a synthetic divisome.

Online content

Any methods, additional references, Nature Portfolio reporting summaries, source data, extended data, supplementary information, acknowledgements, peer review information; details of author contributions and competing interests; and statements of data and code availability are available at https://doi.org/10.1038/s41565-023-01510-3.

References

1. Spira, F. et al. Cytokinesis in vertebrate cells initiates by contraction of an equatorial actomyosin network composed of randomly oriented filaments. *eLife* **6**, e30867 (2017).
2. Allard, J. F. & Cytrynbaum, E. N. Force generation by a dynamic Z-ring in *Escherichia coli* cell division. *Proc. Natl Acad. Sci. USA* **106**, 145–150 (2009).
3. Bisson-Filho, A. W. et al. Treadmilling by FtsZ filaments drives peptidoglycan synthesis and bacterial cell division. *Science* **355**, 739–743 (2017).
4. Pfitzner, A.-K., Moser von Filseck, J. & Roux, A. Principles of membrane remodeling by dynamic ESCRT-III polymers. *Trends Cell Biol.* **31**, 856–868 (2021).
5. Caspi, Y. & Dekker, C. Dividing the archaeal way: the ancient Cdv cell-division machinery. *Front. Microbiol.* **9**, 174 (2018).
6. Bassereau, P. et al. The 2018 biomembrane curvature and remodeling roadmap. *J. Phys. D: Appl. Phys.* **51**, 343001 (2018).
7. Hurley, J. H. ESCRTs are everywhere. *EMBO J.* **34**, 2398–2407 (2015).
8. Sundborger, A. C. & Hinshaw, J. E. Regulating dynamin dynamics during endocytosis. *F1000Prime Rep.* **6**, 85 (2014).
9. Lemus, L. & Goder, V. Membrane trafficking: ESCRTs act here, there, and everywhere. *Curr. Biol.* **32**, R292–R294 (2022).
10. Bohuszewicz, O., Liu, J. & Low, H. H. Membrane remodelling in bacteria. *J. Struct. Biol.* **196**, 3–14 (2016).
11. Olivi, L. et al. Towards a synthetic cell cycle. *Nat. Commun.* **12**, 4531 (2021).
12. Schlimpert, S. et al. Two dynamin-like proteins stabilize FtsZ rings during *Streptomyces* sporulation. *Proc. Natl Acad. Sci. USA* **114**, E6176–E6183 (2017).
13. Bramkamp, M. Structure and function of bacterial dynamin-like proteins. *Biol. Chem.* **393**, 1203–1214 (2012).
14. Guo, L. & Bramkamp, M. Bacterial dynamin-like protein DynA mediates lipid and content mixing. *FASEB J.* **33**, 11746–11757 (2019).
15. Bürmann, F., Ebert, N., van Baarle, S. & Bramkamp, M. A bacterial dynamin-like protein mediating nucleotide-independent membrane fusion. *Mol. Microbiol.* **79**, 1294–1304 (2011).
16. Sawant, P., Eissenberger, K., Karier, L., Mascher, T. & Bramkamp, M. A dynamin-like protein involved in bacterial cell membrane surveillance under environmental stress. *Environ. Microbiol.* **18**, 2705–2720 (2016).
17. Guo, L., Sattler, L., Shafqat, S., Graumann, P. L. & Bramkamp, M. A bacterial dynamin-like protein confers a novel phage resistance strategy on the population level in *Bacillus subtilis*. *mBio* **13**, e0375321 (2022).
18. De Franceschi, N. et al. Synthetic membrane shaper for controlled liposome deformation. *ACS Nano.* **17**, 966–978 (2022).
19. Bhatia, T., Christ, S., Steinkühler, J., Dimova, R. & Lipowsky, R. Simple sugars shape giant vesicles into multispheres with many membrane necks. *Soft Matter* **16**, 1246–1258 (2020).
20. Antonny, B. et al. Membrane fission by dynamin: what we know and what we need to know. *EMBO J.* **35**, 2270–2284 (2016).
21. Mattila, J.-P. et al. A hemi-fission intermediate links two mechanistically distinct stages of membrane fission. *Nature* **524**, 109–113 (2015).
22. Dreher, Y., Jahnke, K., Schröter, M. & Göpfrich, K. Light-triggered cargo loading and division of DNA-containing giant unilamellar lipid vesicles. *Nano Lett.* **21**, 5952–5957 (2021).
23. Steinkühler, J. et al. Controlled division of cell-sized vesicles by low densities of membrane-bound proteins. *Nat. Commun.* **11**, 905 (2020).
24. Kozlovsky, Y. & Kozlov, M. M. Membrane fission: model for intermediate structures. *Biophys. J.* **85**, 85–96 (2003).
25. Fabrikant, G. et al. Computational model of membrane fission catalyzed by ESCRT-III. *PLoS Comput. Biol.* **5**, e1000575 (2009).
26. Zhang, G. & Müller, M. Rupturing the hemi-fission intermediate in membrane fission under tension: reaction coordinates, kinetic pathways, and free-energy barriers. *J. Chem. Phys.* **147**, 064906 (2017).
27. Gao, M., Huang, X., Song, B. L. & Yang, H. The biogenesis of lipid droplets: lipids take center stage. *Prog. Lipid Res.* **75**, 100989 (2019).
28. De Franceschi, N. et al. The ESCRT protein CHMP2B acts as a diffusion barrier on reconstituted membrane necks. *J. Cell Sci.* **132**, jcs217968 (2018).
29. Bertin, A. et al. Human ESCRT-III polymers assemble on positively curved membranes and induce helical membrane tube formation. *Nat. Commun.* **11**, 2663 (2020).
30. Pfitzner, A.-K. et al. An ESCRT-III polymerization sequence drives membrane deformation and fission. *Cell* **182**, 1140–1155.e18 (2020).
31. Schöneberg, J. et al. ATP-dependent force generation and membrane scission by ESCRT-III and Vps4. *Science* **362**, 1423–1428 (2018).
32. Remec Pavlin, M. & Hurley, J. H. The ESCRTs—converging on mechanism. *J. Cell Sci.* **133**, jcs240333 (2020).
33. Abil, Z. & Danelon, C. Roadmap to building a cell: an evolutionary approach. *Front. Bioeng. Biotechnol.* **8**, 927 (2020).
34. Cada, A. K. et al. Friction-driven membrane scission by the human ESCRT-III proteins CHMP1B and IST1. *Proc. Natl Acad. Sci. USA* **119**, e2204536119 (2022).
35. Roux, A., Uyhazi, K., Frost, A. & de Camilli, P. GTP-dependent twisting of dynamin implicates constriction and tension in membrane fission. *Nature* **441**, 528–531 (2006).
36. Tucker, W. C., Weber, T. & Chapman, E. R. Reconstitution of Ca^{2+}-regulated membrane fusion by synaptotagmin and SNAREs. *Science* **304**, 435–438 (2004).
37. Ge, Y. et al. Two forms of Opa1 cooperate to complete fusion of the mitochondrial inner-membrane. *eLife* **9**, e50973 (2020).
38. Bramkamp, M. Bacterial dynamin-like proteins reveal mechanism for membrane fusion. *Nat. Commun.* **9**, 3993 (2018).
39. van de Cauter, L. et al. Optimized cDICE for efficient reconstitution of biological systems in giant unilamellar vesicles. *ACS Synth. Biol.* **10**, 1690–1702 (2021).

Methods

Reagents

Glucose (G7021), $MgCl_2$ (M8266), silicone oil (317667), mineral oil (M3516-1L) and OptiPrep (60% (w/v) iodixanol in water; D1556) were purchased from Sigma-Aldrich. Tris-HCl (10812846001) was purchased from Roche. DOPC (1,2-dioleoyl-*sn*-glycero-3-phosphocholine) (850375), DOPE-PEG(2000) amine (1,2-dioleoyl-*sn*-glycero-3-phosphoethanolamine-*N*-[amino(polyethylene glycol)-2000] (ammonium salt)) (880234), 18:1 (Δ9-Cis) PG (1,2-dioleoyl-*sn*-glycero-3-phospho-(1′-*rac*-glycerol) (sodium salt)) (840475) and DOPE-rhodamine (1,2-dioleoyl-*sn*-glycero-3-phosphoethanolamine-*N*-(lissamine rhodamine B sulfonyl) (ammonium salt)) (810150C) were purchased from Avanti Lipids. Lipids were stored and resuspended in anhydrous chloroform (288306, Sigma-Aldrich). UltraPure bovine serum albumin used for the passivation of glass coverslips was purchased from Thermo Fisher. For the FRAP experiments on a soluble dye, Alexa Fluor 488 C5 maleimide was used (A10254, Thermo Fisher). Extended Data Table 1 lists the composition of solutions used in SMS preparations.

DNA constructs

The four DNA oligos comprising the cross-shaped nanostars were purchased from IDT. The sequence of DNA oligos comprising the nanostars and cholesterol–oligo are reported elsewhere[18].

Protein purification and labelling

DynA from *B. subtilis* was overexpressed from pET16b (kindly provided by M. Bramkamp) and purified essentially as described[15], but eluted with a linear imidazole gradient instead of a step elution. A solution of ~10 µM dynamin was labelled with an eightfold molar excess of Alexa Fluor 488 maleimide in the presence of 0.05 mM TCEP (45 min at room temperature), quenched with 10 mM β-mercaptoethanol and separated from free label on a Superdex S200 column equilibrated with T5 buffer (50 mM Tris-HCl pH 8.0, 500 mM NaCl, 10% glycerol). DynA–D1 (residues 1-609) and DynA–D2 (residues 561-1193) domains were cloned in the pET16b vector. Purification and labelling was done as for the wild-type DynA.

Lipid-in-oil suspension and droplet preparation

Lipid-in-oil suspensions were prepared according to another work[18]. Briefly, lipids solubilized in chloroform were mixed and blow-dried. They were resolubilized with chloroform inside a glovebox, and a mixture of silicone and mineral oil[39] was added. The resulting suspension was sonicated in ice for 15 min. The lipids mix used in this study was composed of DOPC (89.75% mol/mol), DSPE-PEG2000-biotin (2.00% mol/mol), DOPG (8.00% mol/mol) and DOPE-rhodamine (0.25% mol/mol).

Dumbbell preparation

Dumbbell liposomes were prepared using the SMS approach[18]. In this technique, droplets were generated by pipetting an 'inner' aqueous solution into a lipid-in-oil suspension that was subsequently placed on top of a water reservoir, referred to as the 'outer' buffer. Liposomes were then formed when the droplets crossed the oil-to-water interface (between oil and outer buffer) as they slowly sank due to gravity. Small (96.5 kDa) DNA structures called nanostars (which basically are Holliday junctions armed with cholesterol moieties, collectively referred to as 'CN') were present in the outer solution bound to the outer membrane during liposome formation. The hyperosmotic outer solution caused osmotic deflation and thus high membrane deformability, whereas CN binding induced a positive membrane curvature, which led to a high yield of dumbbell-shaped liposomes. The inner buffer was composed of 50 mM Tris pH 7.5 + 37% OptiPrep. The outer buffer was composed of 50 mM Tris pH 7.5 + 5 mM $MgCl_2$, to which glucose was added until reaching an osmolarity 40 mOsm higher than the inner buffer. Also, 250 nM of each of the four oligomers comprising the nanostars and 1 µM of cholesterol–oligo[18] were added to the outer buffer. DynA at 100 nM was added to the inner buffer; droplets were generated by manual pipetting and they were added to the outer buffer. For the experiment shown in Supplementary Fig. 5a,c, the DynA concentration of 20 nM was used to minimize aggregation and to obtain dumbbells[18].

Data collection and analysis

Fluorescence images were acquired at the midplane of liposomes using spinning-disc confocal laser microscopy (Olympus IX81 microscope, ×60 objective, iXon camera) with Andor iQ3 software. To induce photobleaching, we employed raster scanning with a 491 nm laser (at 9.8 mW) over the region of interest. To measure the recovery signal, frames were collected every 1 s, starting right after the photobleaching event. Fluorescence images were analysed and processed using ImageJ (v. 2.1.0). The extracted fluorescence data were plotted and fitted using Python 3. Supplementary Note 1 provides a detailed explanation of the image analysis pipeline.

Statistics and reproducibility

Statistical analysis of the data was performed as indicated in the figure captions. No statistical method was used to predetermine the sample size. Criteria for excluding data points (that is, individual necks within a chain of dumbbells) during image acquisition were (1) the presence of lipid clusters at the neck, (2) convoluted chains of dumbbells that precluded the visual determination of connectivity between lobes and (3) lobes smaller than ~3 µm that precluded accurate bleaching. In the plot shown in Fig. 4f, two outliers with value more than 160 were excluded.

Calculation of R_R

The R_R value at the membrane necks was calculated using the following formula:

$$S = \frac{I^{\text{protein}}_{\text{neck}} - I^{\text{protein}}_{\text{background}}}{I^{\text{protein}}_{\text{GUV lumen}} - I^{\text{protein}}_{\text{background}}},$$

where $I^{\text{protein}}_{\text{neck}}$ and $I^{\text{protein}}_{\text{GUV lumen}}$ represent the fluorescence intensities of the protein at the neck and of the residual protein present in the lumen of the liposome, respectively.

Estimation of neck diameter

The neck diameter (Extended Data Fig. 6c) was estimated as detailed elsewhere[18]. Briefly, we encapsulated a small soluble dye (Alexa 647) inside the lumen of dumbbells in the presence or absence of DynA. We then photobleached the soluble dye present in the lumen of one lobe and recorded the dye fluorescence as it recovered from the other lobe via the open neck. These recovery curves were fitted using a diffusion model[18], yielding an estimation of the neck size.

Data availability

The data that support the findings of this study are available within the paper and its Supplementary Information. Other relevant data are available from the corresponding author on reasonable request. Source data are provided with this paper.

Code availability

The image analysis source code is available via Zenodo at https://zenodo.org/record/8056488.

Acknowledgements

We thank S. J. Marrink and W. Pezeshkian for useful discussions, and M. Bramkamp for kindly providing the plasmid for *B. subtilis* DynA. We acknowledge funding support from the BaSyC program of NWO-OCW, from ERC Advanced Grant 883684 and from Regenerative Mechanisms for Health—ReMedy project MAB/2017/2.

Author contributions

C.D., N.D.F. and S.M. designed the study. N.D.F. and C.D. designed the experiments. N.D.F. and S.M. carried out the experiments. N.D.F., R.B. and A.F. analysed the data. C.D. supervised the study. C.D. and N.D.F. wrote the manuscript with input from all other authors. All the authors provided critical feedback on the research and the manuscript.

Competing interests

The authors declare no competing interests.

Additional information

Extended data is available for this paper at https://doi.org/10.1038/s41565-023-01510-3.

Supplementary information The online version contains supplementary material available at https://doi.org/10.1038/s41565-023-01510-3.

Correspondence and requests for materials should be addressed to Cees Dekker.

Peer review information *Nature Nanotechnology* thanks Gerhard Gompper, Oskar Staufer and the other, anonymous, reviewer(s) for their contribution to the peer review of this work.

https://doi.org/10.1038/s41565-023-01510-3

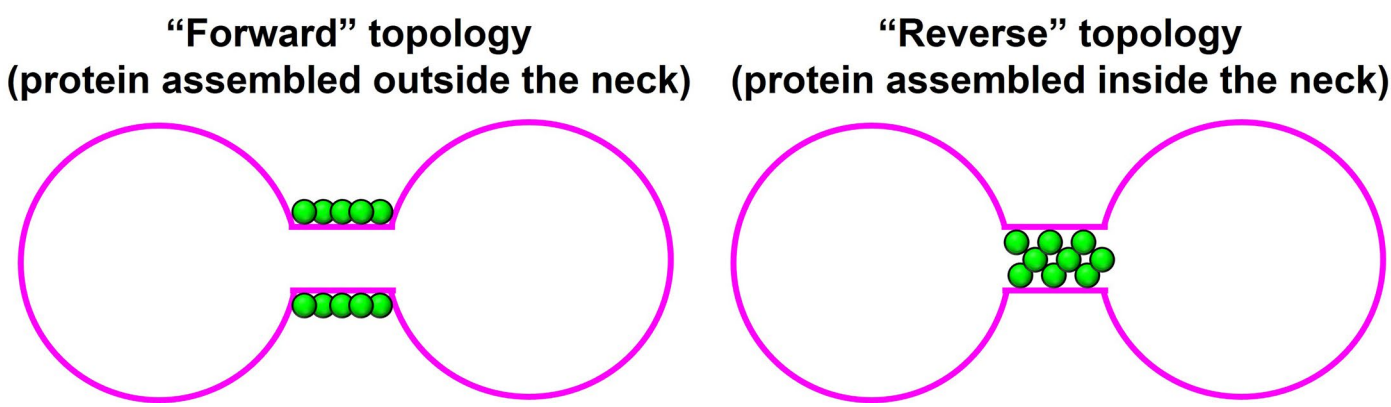

Extended Data Fig. 1 | Membrane topologies. Relative positions of membrane and protein machinery for the forward and reverse topology. The membrane is in magenta, proteins are in green.

https://doi.org/10.1038/s41565-023-01510-3

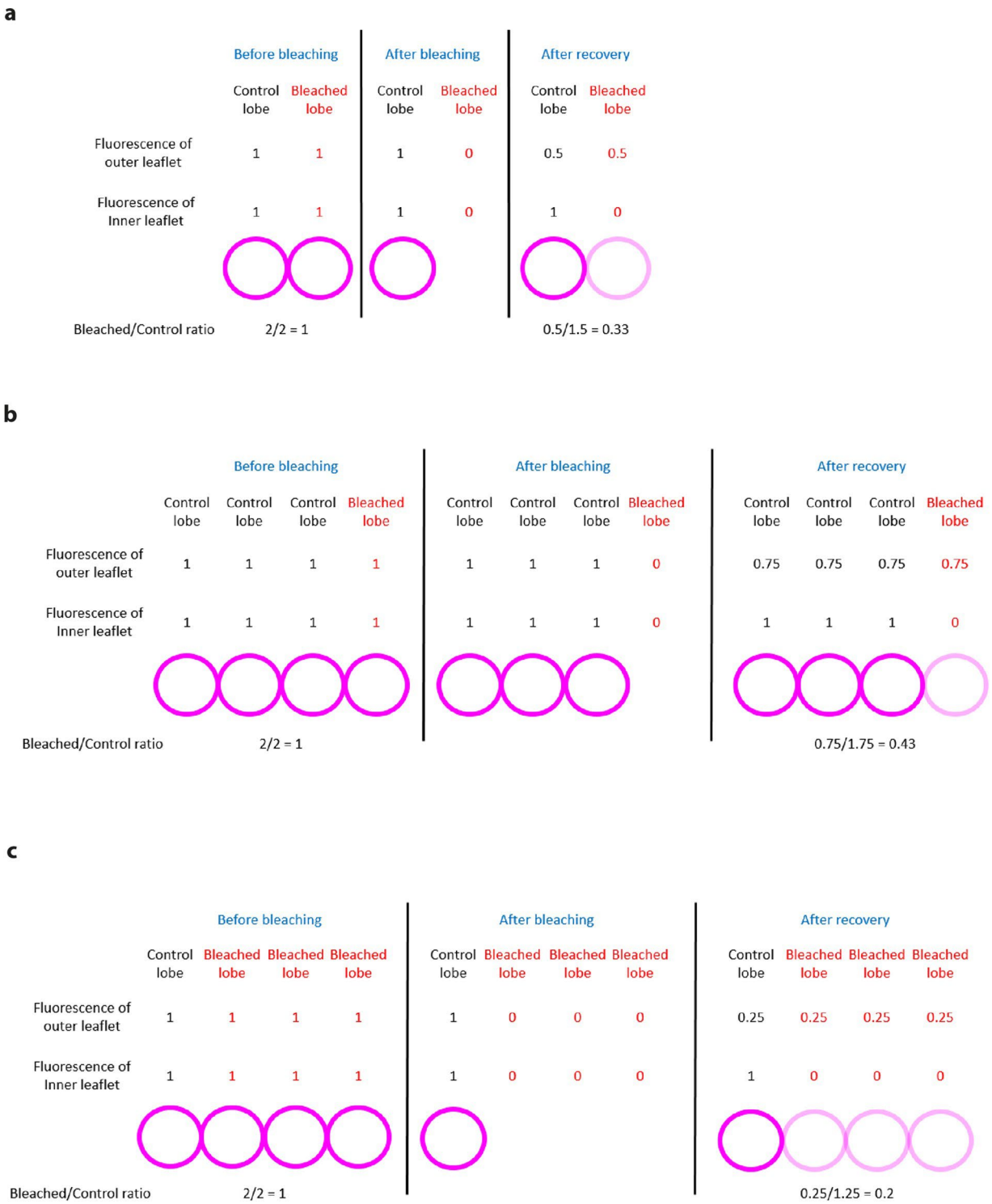

Extended Data Fig. 2 | Schematic depicting the expected values of N_t. Schematic depicting the expected values of N_t for different amounts of membrane reservoir in control and bleached lobes. (**a**) equal amount; (**b**) larger reservoir in control lobe; (**c**) larger reservoir in the bleached lobe.

https://doi.org/10.1038/s41565-023-01510-3

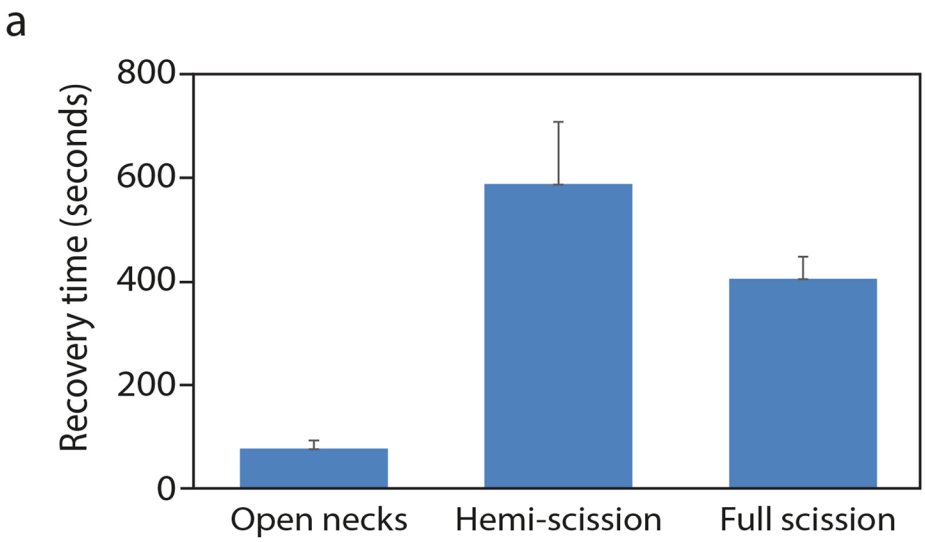

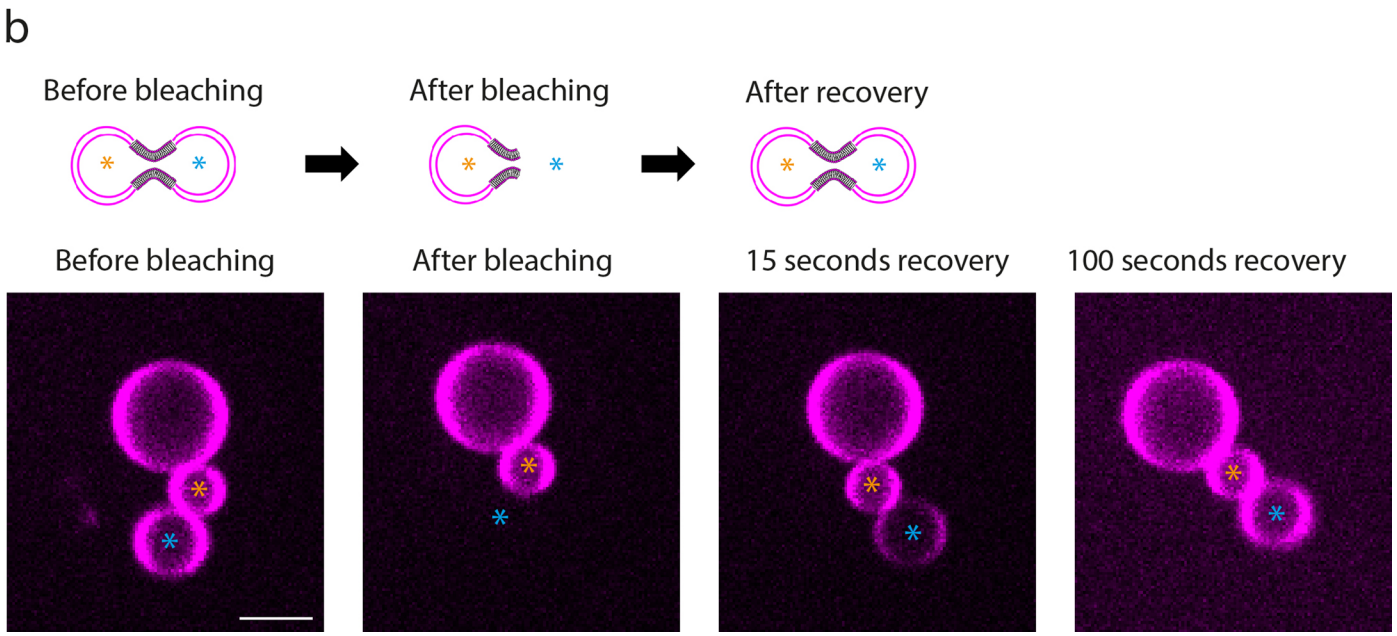

Extended Data Fig. 3 | Recovery times in FRAP experiments and example of open neck in the absence of DynA. (**a**) Median of the duration of recovery times in FRAP experiments. Acquisition was stopped when no further lipid recovery was apparent. This quantitation is obtained from datasets such as shown in Fig. 2a,b and Supplementary Fig. 5b. n = 190 necks from 24 independent experiments. Data are presented as median values +/− SEM. (**b**) example of FRAP experiment showing full lipid recovery (open neck) on a chain of dumbbells without reconstitution of DynA. The orange asterisk indicates the control lobe, the blue asterisk indicates the bleached lobe. Scale bar: 5µm.

https://doi.org/10.1038/s41565-023-01510-3

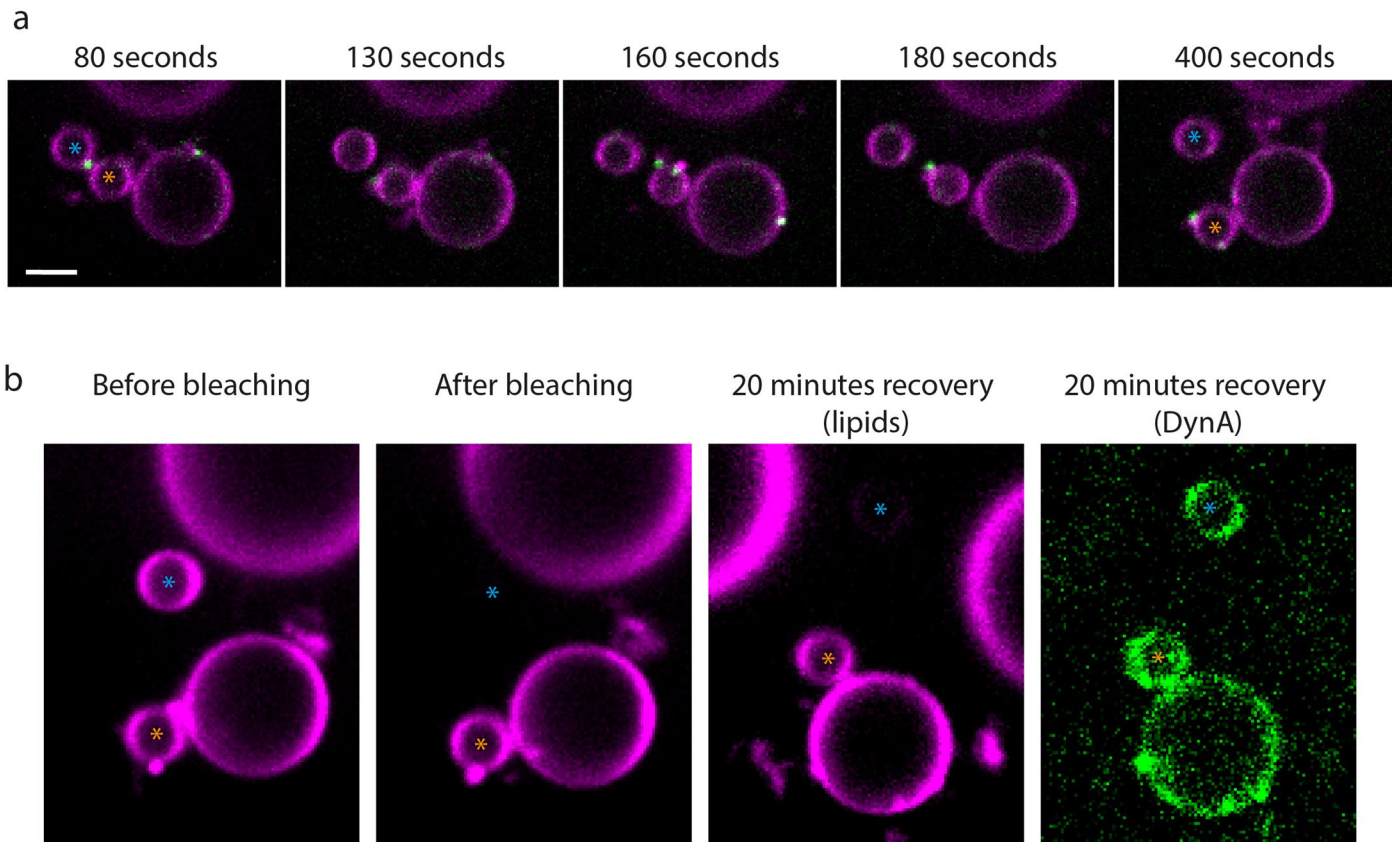

Extended Data Fig. 4 | Lobe detachment upon scission. (**a**) Confocal images of a dumbbell with a DynA cluster (in green) localized at neck. The dumbbell was imaged just as scission was occurring and the two lobes are drifting apart. (**b**) same dumbbell as in panel a. After lobes separation, FRAP analysis confirmed that the membrane connection between the two lobes had been lost and that no lipid recovery occurred. The bleached lobe is indicated by a blue asterisk, and its position is revealed by the low fluorescent signal of DynA binding to the membrane in the overexposed image.

https://doi.org/10.1038/s41565-023-01510-3

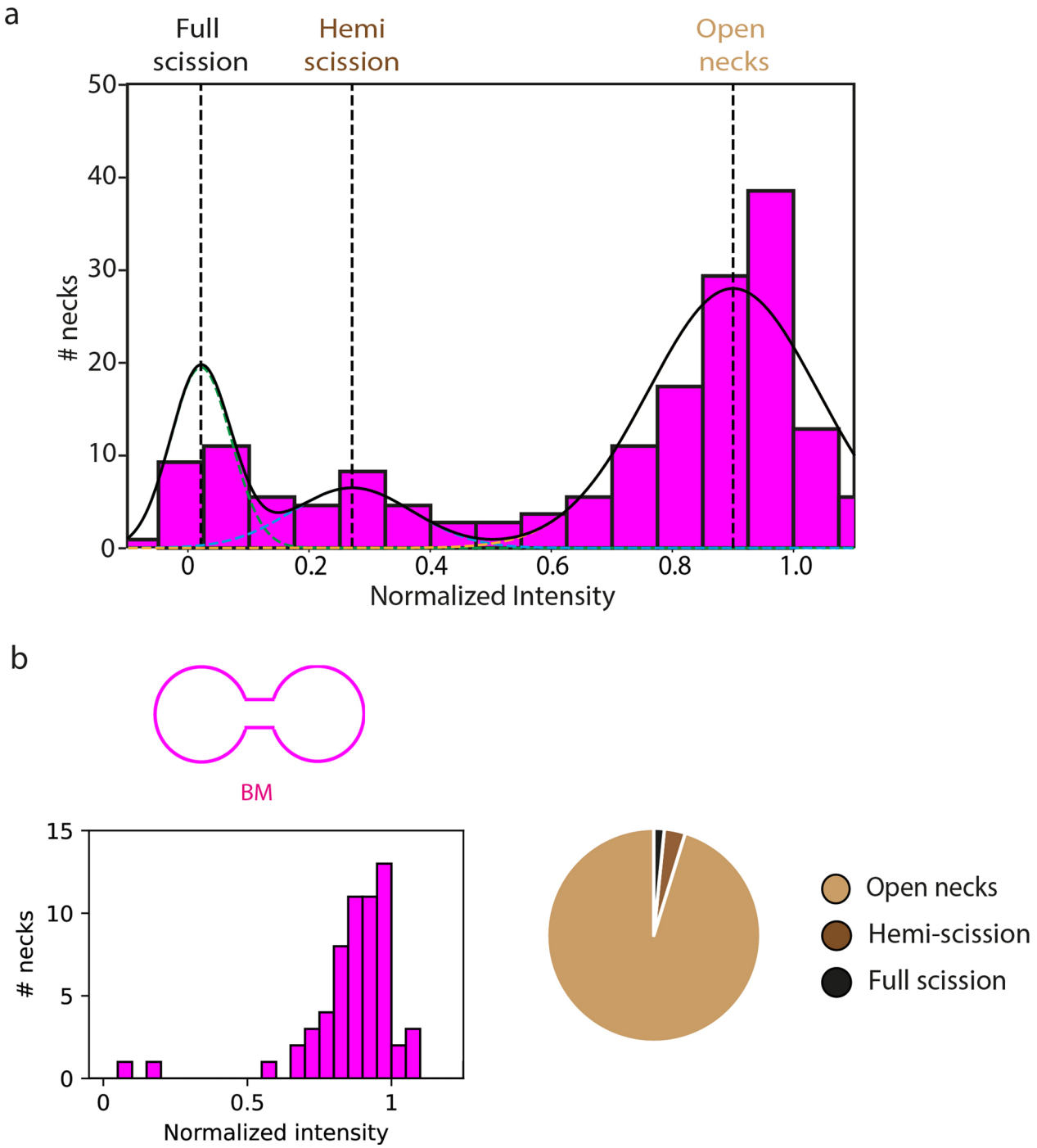

Extended Data Fig. 5 | Quantification of the N_t in different experimental conditions. (**a**) Quantification of the N_t of a large dataset of necks from chains of dumbbells. This plot shows the data pooled from the three experimental conditions shown in Fig. 2a,b and Supplementary Fig. 6b (n = 190 chains of dumbbells), and are decomposed into three peaks using a Gaussian Mixture Model. The three peaks correspond to open necks, hemi-scission and full scission. For each data point, the fluorescent lipids of one lobe were bleached and their recovery was followed over time until reaching the plateau. The final intensity was used for calculating and plotting the N_t. (**b**) Plot showing the N_t of dumbbells having only bare membrane (left), and pie-chart (right) indicating the fraction of open necks, hemi-scission and full scission events (BN; 63 necks from 5 independent preparations).

https://doi.org/10.1038/s41565-023-01510-3

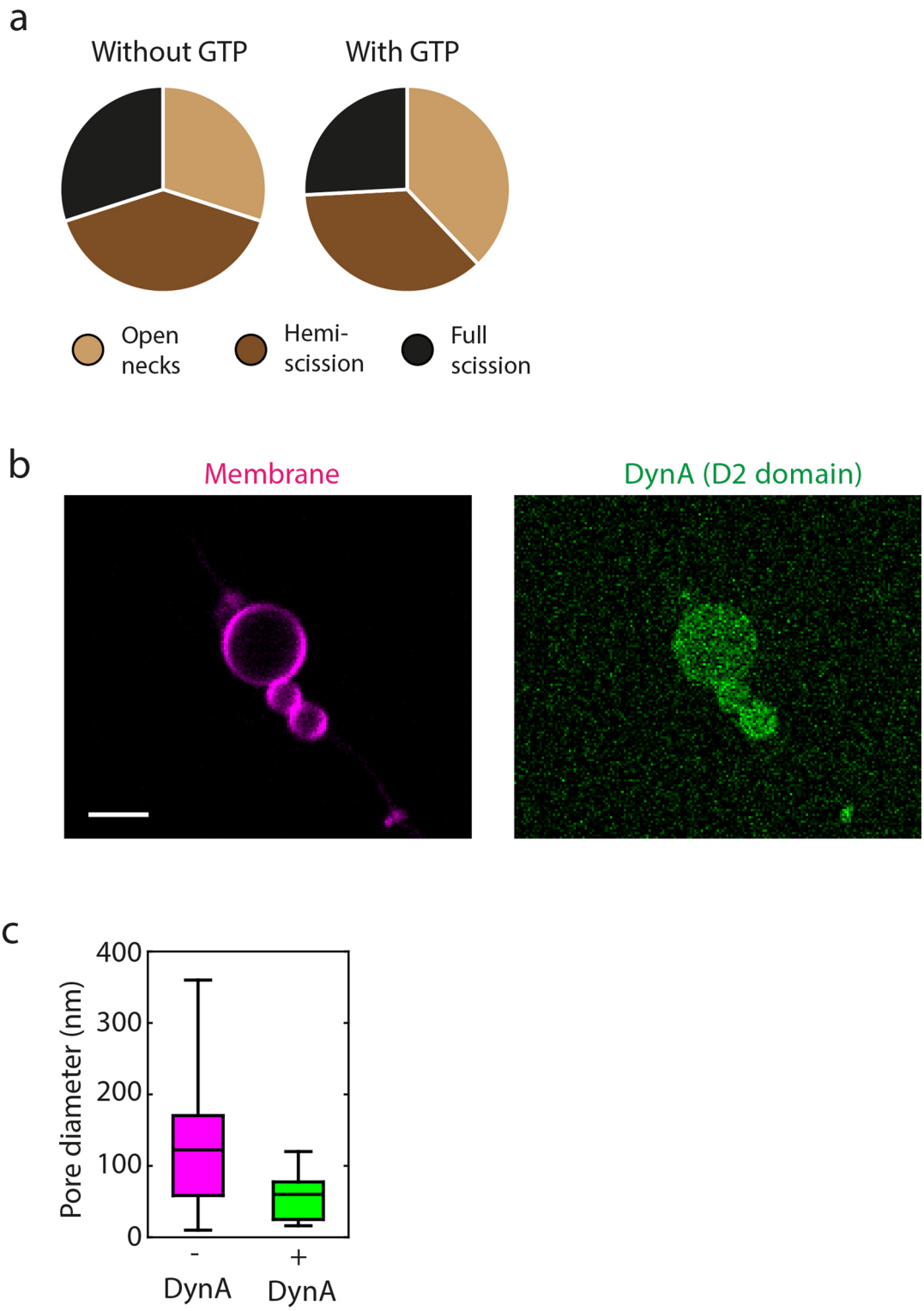

Extended Data Fig. 6 | Membrane remodelling by DynA in different experimental conditions. (**a**) pie-charts indicating the fraction of open necks, hemi-scission and full scission events in the presence or absence of GTP. Both samples include cholesterol-oligo, CN and DynA. With GTP, n = 59; without GTP n = 10. (**b**): lack of binding of DynA-D2 domain to membrane containing 7.5% DOPG in the absence of Mg^{++}. Scale bar: 5µm. (**c**) DynA assembly at the neck results in neck constriction. The plot shows the neck diameter in the presence or absence of DynA, estimated based on dye recovery upon photobleaching. In open necks and in the absence of DynA, the average inner diameter of necks was 134 ± 108 nm (mean ± SD). In the presence of DynA, the width of open necks appeared more constricted, with an average diameter of 57 ± 33 nm (mean ± SD). n = 8 without DynA; n = 9 with DynA. The estimation has been performed according to the procedure detailed in Ref. 18.

https://doi.org/10.1038/s41565-023-01510-3

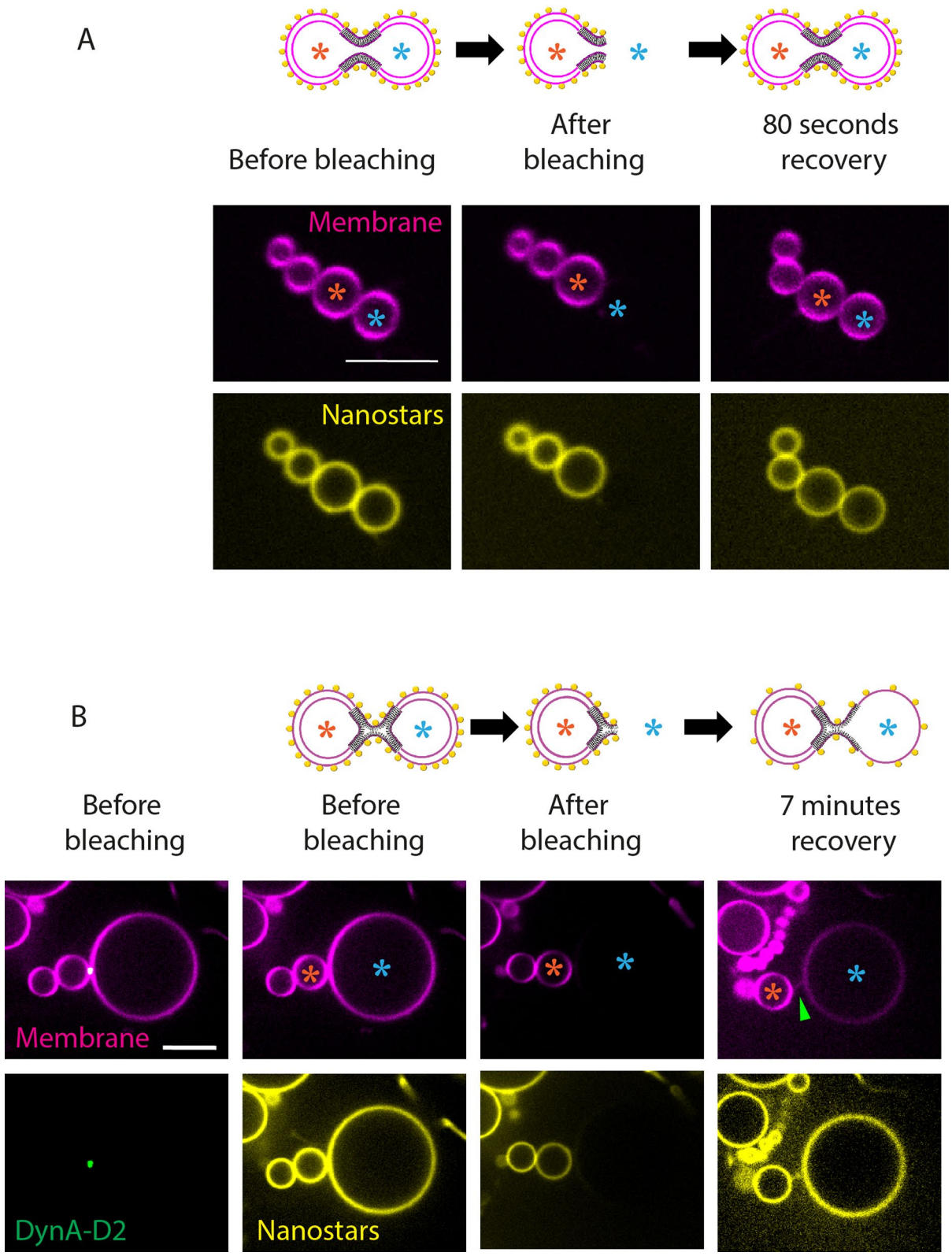

Extended Data Fig. 7 | Recovery in hemi-scission state is achieved via the outer leaflet. (**a**) Full recovery of both fluorescent lipids (which are in both leaflets of the bilayer) and fluorescent nanostars (which attach to the outer leaflet only) upon photo-bleaching of a dumbbell liposome having an open neck (without DynA). Scale bar: 5μm. (**b**) Partial recovery of fluorescent lipids and full recovery of fluorescent nanostars upon photo-bleaching of a dumbbell liposome with a DynA-D2 cluster. The neck is in a hemi-scission state, as visualized by the partial lipid recovery. The green arrowhead indicates the position of the neck connecting the two lobes. Scale bar: 10μm.

https://doi.org/10.1038/s41565-023-01510-3

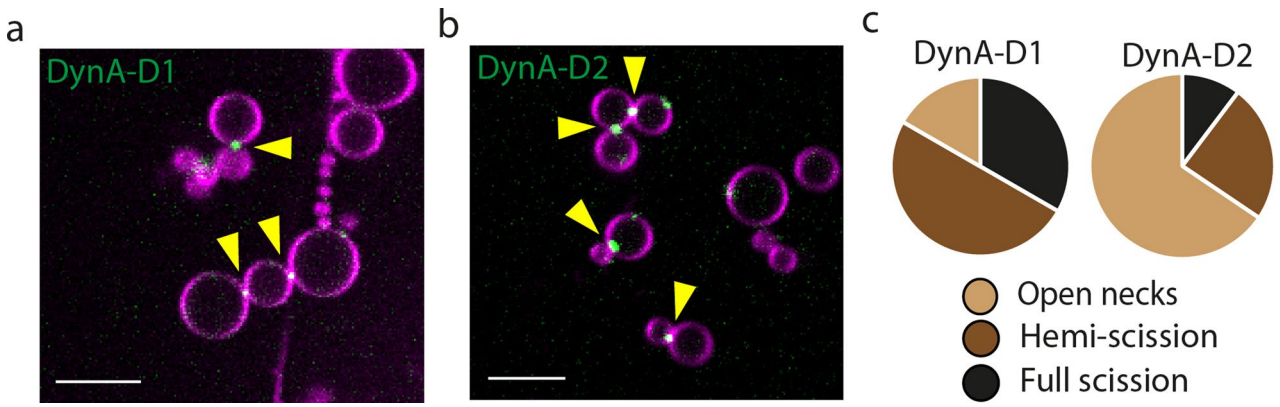

Extended Data Fig. 8 | Membrane remodelling by Dyna-D1 and DynA-D2 domains. (**a**) DynA-D1 domain reconstituted at necks of dumbbell liposomes. (**b**) DynA-D2 domain reconstituted at necks of dumbbell liposomes. Arrowheads indicate protein clusters localized at necks. Scale bars: 10µm. (**c**) Pie-charts indicating the fraction of open necks, hemi-scission, and full scission events upon reconstitution of DynA D1 and D2 domains. n = 12 necks from 3 independent preparations (D1); n = 27 from 3 independent preparation (D2).

https://doi.org/10.1038/s41565-023-01510-3

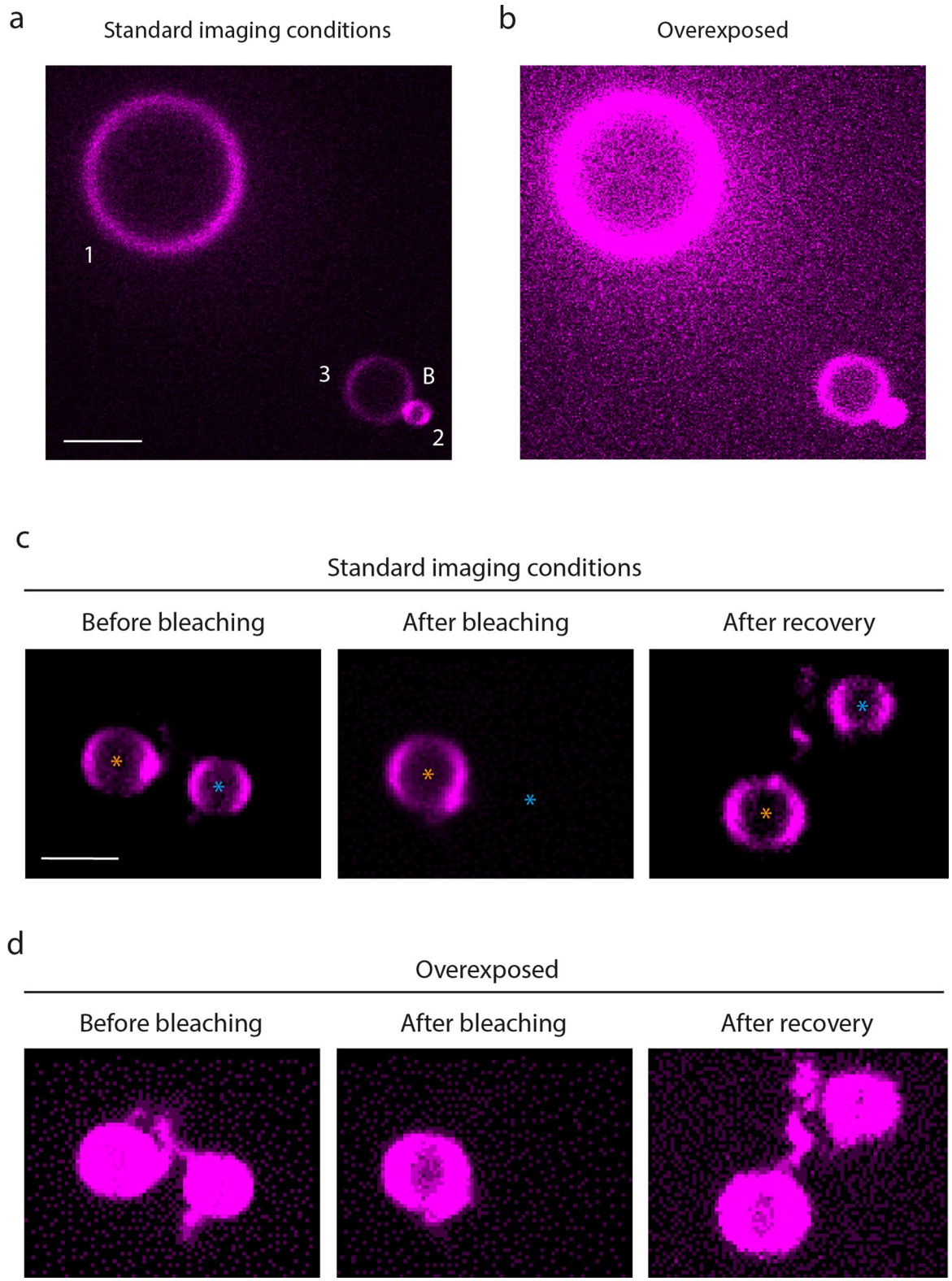

Extended Data Fig. 9 | Lobe detachment upon scission and visualization of nanotube. (**a**) confocal image of liposomes that underwent full scission (identical to Fig. 4e). (**b**) Same image as in (a) but with increased gain, causing overexposure of the liposome membrane. This condition confirms that the two lobes indeed underwent scission, since no nanotube is visibly connecting the two liposomes. Note that in panel d, a nanotube was visible upon overexposure. Scale bar: 10µm. (**c**) Confocal image of two liposomes under standard imaging conditions which allow to clearly see the liposome membrane without overexposure. Upon bleaching of one liposome (marked with a blue asterisk) full lipid recovery could be observed. (**d**) Same images as in panel c with increased gain, causing overexposure of the liposome membrane. Such conditions reveal that a membrane nanotube is connecting the two liposomes and allows full lipid recovery. Scale bar: 5µm.

https://doi.org/10.1038/s41565-023-01510-3

Extended Data Table 1 | Composition of inner and outer solutions

	Inner Solution	Outer Solution
Tris-HCl pH 7.5	50 mM	50 mM
$MgCl_2$	5 mM	5 mM
Optiprep	37 %	-
Recombinant DynaminA	100 nM	-
Glucose	-	To adjust osmolarity
Nanostars (CN)	-	250 nM

Composition of the inner and outer solutions used in this study. The osmolarity of the outer solution was adjusted using glucose in order to be 40 mOsm higher than the osmolarity of the inner solution.